Chemical Science

ROYAL SOCIETY OF CHEMISTRY

EDGE ARTICLE

View Article Online
View Journal | View Issue

Check for updates

Cite this: *Chem. Sci.*, 2024, **15**, 18085

All publication charges for this article have been paid for by the Royal Society of Chemistry

Spotting d-band centers of single-atom catalysts by oxygen intermediate-boosted electrochemiluminescence†

Ruyu Xie,[a] Kaitao Li,[ac] Rui Tian*[ac] and Chao Lu *[abc]

Catalytic activities of single-atom catalysts are strongly dependent on their d-band centers. However, it is a long-standing challenge to provide a cost-effective and accurate evaluation for the positions of d-band centers of these catalysts due to the fact that the widely applicable photoelectron spectroscopy methodologies require complicated sampling and spectral unfolding processes. In this contribution, we have proposed oxygen intermediate-boosted electrochemiluminescence (ECL) for rapid spotting of the d-band centers of single-atom catalysts, involving single atomic Au, Ag, Cu and Fe. It was disclosed that the d-band centers of single-atom catalysts closer to the Fermi level could facilitate the interaction between catalysts and oxygen intermediates, leading to higher luminol ECL intensities as a result of the promoted adsorption and reduction ability towards oxygen intermediates. Moreover, this correlation was also adapted for other metal catalysts such as Au and Ag nanoparticles. This correspondence could be utilized for an accurate identification of d-band centers of single-atom catalysts. It is anticipated that the proposed strategy could be beneficial for a deep understanding of microstructure studies of single-atom catalysts to achieve advanced catalytic performances.

Received 8th June 2024
Accepted 7th October 2024

DOI: 10.1039/d4sc03763d

rsc.li/chemical-science

Open Access Article. Published on 07 October 2024. Downloaded on 2/8/2026 9:26:34 AM.
This article is licensed under a Creative Commons Attribution-NonCommercial 3.0 Unported Licence.

Introduction

The d-band model for single-atom catalysts highlights the role of the electronic states in the valence band in influencing the reaction activity.[1] To unravel the factors that govern the catalytic activities of single-atom catalysts, the positions of their d-band centers have been studied as a descriptor for the modulation of the electronic structure.[2] The position of d-band centers could determine the hybridization energy between the bonding and antibonding states of oxygen intermediates and d-bands of single atoms.[1] As the d-band center shifts up, more antibonding states are pulled above the Fermi level,[3] lowering the energy barrier and facilitating the oxygen reduction reaction.[4,5] To achieve high-efficiency catalytic performances, increasing efforts have been devoted to engineering the d-band centers of single-atom catalysts.[6–8] For example, the single-atom catalysts could be anchored on a specific support through the coordination interaction, and the electronic metal–support interactions (EMSI) contributed to the redistributed electrons, modulated d-band centers and thereby boosted catalytic activities.[9,10] Therefore, it is critically important to identify the positions of d-band centers of single-atom catalysts to reveal the electronic structure–activity relationship.

To evaluate the positions of the d-band centers of single-atom catalysts, the general strategies relied on photoelectron spectroscopy methodologies, such as X-ray photoelectron spectroscopy (XPS)[11,12] and ultraviolet photoelectron spectroscopy (UPS).[13] However, the detection depth of XPS measurements is on the nanometer scale, failing to provide comprehensive information on the electronic structure of catalysts.[14,15] UPS showed high requirements for samples, of which the surface should be fresh and free from contamination. In addition, the density functional theory calculations to study the structure of catalysts are time-consuming and demand extensive theoretical knowledge.[16] These strategies are hardly accessible as widely applicable methodologies for the studies on single-atom catalysts. Therefore, it is highly desirable to explore a sensitive and feasible strategy to identify the d-band centers of single-atom catalysts and provide an in-depth recognition of the variations of the electronic structure during the reactions.

Electrochemiluminescence (ECL), a kind of chemiluminescence triggered by electrochemical reactions, has been known for its inherent advantages of low background signal, cost-effectiveness and high sensitivity.[17,18] Specifically, the electrochemical oxidation of luminol involves the reaction of reactive oxygen species (ROS) and contributes to the oxygen intermediate-boosted ECL signals.[19,20] These features make ECL

[a]State Key Laboratory of Chemical Resource Engineering, Beijing University of Chemical Technology, Beijing 100029, China. E-mail: tianrui@mail.buct.edu.cn; luchao@mail.buct.edu.cn

[b]Pingyuan Laboratory, College of Chemistry, Zhengzhou University, Zhengzhou, 450001, China

[c]Quzhou Institute for Innovation in Resource Chemical Engineering, Quzhou, 324000, China

† Electronic supplementary information (ESI) available. See DOI: https://doi.org/10.1039/d4sc03763d

© 2024 The Author(s). Published by the Royal Society of Chemistry

Open Access Article. Published on 07 October 2024. Downloaded on 2/8/2026 9:26:34 AM. This article is licensed under a Creative Commons Attribution-NonCommercial 3.0 Unported Licence.

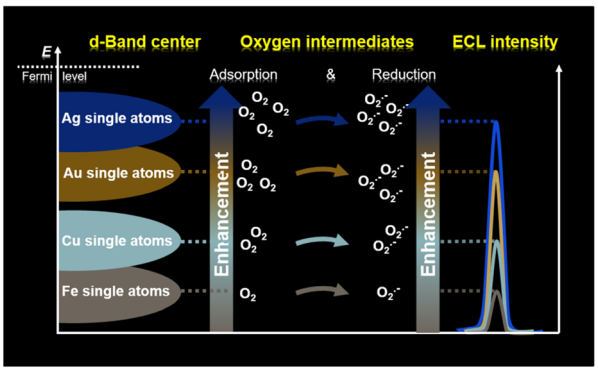

Scheme 1 Schematic illustration of ECL to spot the positions of d-band centers of single-atom catalysts.

a promising strategy for identifying both the quantities and reaction behaviors of oxygen intermediates, thereby allowing the evaluation of the d-band centers of single-atom catalysts. In this work, we have localized the Ag, Au, Cu and Fe single atoms on a two-dimensional layered double hydroxide (LDH) support on ITO glass (referred to as Ag^{s}/LDH/ITO, Au^{s}/LDH/ITO, Cu^{s}/LDH/ITO, and Fe^{s}/LDH/ITO), and the varied d-band centers of these single-atom catalysts were identified through the luminol ECL intensities (Scheme 1). This is because the upshifted d-band centers towards the Fermi levels of these single-atom catalysts are apt to create favorable binding interactions between catalysts and oxygen intermediates, resulting in the facilitated adsorption and reduction kinetics of oxygen intermediates. Accordingly, the oxygen intermediate-boosted ECL signals of these single-atom catalysts conformed to the same tendency as the positions of d-band centers relative to the Fermi level: Ag^{s}/LDH/ITO > Au^{s}/LDH/ITO > Cu^{s}/LDH/ITO > Fe^{s}/LDH/ITO. Moreover, this study was extended to Ag and Au nanoparticles. The results showed the higher catalytic performance of Ag species than Au species, and the promoted atomic utilization of single atoms compared to that of nanoparticles was also validated. Therefore, we have proposed intermediate-boosted ECL as a sensitive and cost-effective approach to spot the d-band centers of single-atomic and metallic catalysts. It is anticipated that our strategy would provide valuable information for the study and modulation of the electronic structures of catalysts.

Results and discussion

Correlation between the d-band centers and ECL intensities

CoAl/LDH, featuring the two-dimensional structural characteristics of LDHs and the catalytically active Co element, was employed as a support to localize different kinds of catalysts.[21,22] CoAl/LDH was prepared on an ITO electrode through a hydrothermal method. To localize the different metal species with varied d-band centers onto LDH/ITO, electrochemical deposition was employed. The structure of the localized metal was highly dependent on the mass loadings of the metal species during the electrochemical deposition, corresponding to the minimum supersaturation on the support.[23] In detail, single atomic Au and Ag were anchored onto the LDH/ITO electrodes through the electrochemical deposition for 2 cycles (denoted as Ag^{s}/LDH/ITO and Au^{s}/LDH/ITO), and the contents of Au and Ag were determined to be 0.071 mol% and 0.077 mol% by inductively coupled plasma optical emission spectrometry. The referenced Au and Ag nanoparticles were electrochemically deposited on the LDH/ITO electrodes after 30 cycles (labelled as Au^{np}/LDH/ITO and Ag^{np}/LDH/ITO), with the contents of Au and Ag of 0.214 mol% and 0.226 mol%. The d-band centers relative to the Fermi level of these catalysts were studied by implementing the highly surface-sensitive ultraviolet photoelectron spectroscopy (UPS). The UPS valence-band spectra showed that the energy of d-band centers of Ag^{s}/LDH/ITO was located at −4.24 eV, which was higher than that of −4.33 eV for Au^{s}/LDH/ITO (Fig. 1a). Furthermore, the values of d-band centers of Ag^{np}/LDH/ITO and Au^{np}/LDH/ITO were determined to be −4.45 eV and −4.54 eV, respectively. It could be concluded that more shifts towards the Fermi level could be acquired for the d-band centers of single atoms than those of the nanoparticles, which could be attributed to the larger proportion of low coordinated atoms in the nanoparticles.[24] Moreover, Ag species shared the higher d-band center values than Au did, and this phenomenon could be explained by the electron distribution of different metal species.[2] Concretely, the values of the d-band centers of these modified electrodes followed the trend of Ag^{s}/LDH/ITO > Au^{s}/LDH/ITO > Ag^{np}/LDH/ITO > Au^{np}/LDH/ITO. According to the d-band theory proposed by Nørskov, the upshifts of d-band centers would result in the variations of antibonding states,[25] leading to the strong adsorption strength towards intermediates and facilitating the rate-limiting reactions for the catalytic reactions.

The ECL performances of these modified electrodes were recorded in a 0.01 mmol L^{-1} luminol solution (0.1 mol L^{-1}

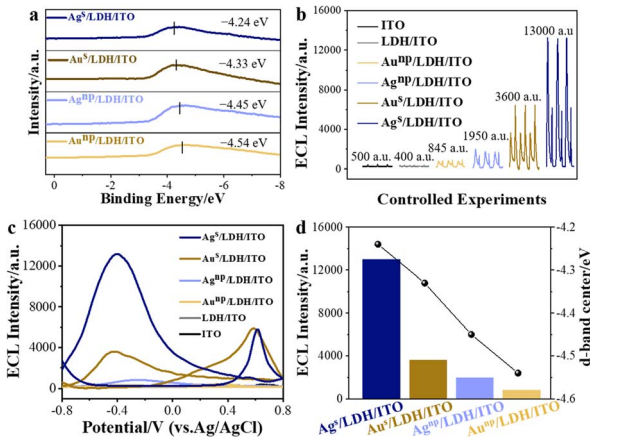

Fig. 1 (a) UPS valence-band spectra of Ag^{s}/LDH/ITO, Au^{s}/LDH/ITO, Ag^{np}/LDH/ITO, and Au^{np}/LDH/ITO relative to the Fermi level; the black solid lines represent the positions of the d-band centers; (b) ECL intensities and (c) I_{ECL}–potential curves for ITO, LDH/ITO, Au^{np}/LDH/ITO, Ag^{np}/LDH/ITO, Au^{s}/LDH/ITO and Ag^{s}/LDH/ITO in 0.01 mmol per L luminol (PBS, pH = 7.5); (d) correlation between the d-band centers and ECL intensities of Ag^{s}/LDH/ITO, Au^{s}/LDH/ITO, Ag^{np}/LDH/ITO, and Au^{np}/LDH/ITO electrodes (the values of d-band centers were measured by UPS as shown in (a).

© 2024 The Author(s). Published by the Royal Society of Chemistry

Open Access Article. Published on 07 October 2024. Downloaded on 2/8/2026 9:26:34 AM. This article is licensed under a Creative Commons Attribution-NonCommercial 3.0 Unported Licence.

phosphate buffered saline, pH = 7.5) over a voltage range of −0.8 to 0.8 V (Fig. 1b). No obvious ECL signals could be observed on the bare ITO or LDH/ITO electrodes. Upon the deposition of single atomic Au or Ag, the modified electrodes showed the prominently promoted ECL intensities. The cathodic luminol ECL intensity of Ag^{s}/LDH/ITO was about 13 000 a.u., while that of Au^{s}/LDH/ITO was only 3600 a.u. In comparison with the localized single atoms, Ag^{np}/LDH/ITO and Au^{np}/LDH/ITO with downshifted d-band centers showed less effect on promoting the ECL signals, with the ECL intensities of 1950 a.u. and 845 a.u., respectively. The I_{ECL}–potential and synchronous cyclic voltammetry (CV) curves of different modified electrodes were recorded for validation. An anodic ECL peak at +0.6 V appeared for both Ag^{s}/LDH/ITO and Au^{s}/LDH/ITO electrodes during the positive scan, and the cathodic ECL peak at −0.4 V was noted during the negative scan for these electrodes (Fig. 1c). The ECL spectra recorded at the cathode showed a maximum emission wavelength of around 425 nm (Fig. S1†), validating the emissive species as the excited 3-aminophthalate dianion from luminol.[26] The CV curve of Ag^{s}/LDH/ITO showed a broad oxidation peak at +0.45 V during the positive scan (Fig. S2†), which was correlated to the oxidation of $Ag^{\delta+}$ and luminol.[27] During the reversed potential scan, the reduction reactions of Ag^{+} and dissolved oxygen were found at −0.005 V and −0.55 V, respectively.[28] For Au^{s}/LDH/ITO, the reduction of the oxidized gold could be observed at +0.03 V, and the oxidation process of luminol was identified at +0.58 V.[29,30] In comparison, the peaks at the cathode during the negative scanning potential, which were associated with the reduction of the oxidized metal species and the dissolved oxygen,[31] were more pronounced for Ag^{s}/LDH/ITO than for the Au^{s}/LDH/ITO electrode. These results demonstrated that single atomic Ag showed a stronger oxygen adsorption capacity to reduce oxygen to generate intermediate radical species. These superior behaviors of Ag^{s}/LDH/ITO could be reflected by the ECL due to its ultrasensitive features to interpret the subtle changes during an electrochemical reaction.[32]

It should be noted that the ECL intensities were highly correlated with the positions of d-band centers of the modified electrodes. The trends for the d-band centers relative to the Fermi level of Ag^{s}/LDH/ITO, Au^{s}/LDH/ITO, Ag^{np}/LDH/ITO, and Au^{np}/LDH/ITO are in good accordance with the tendencies of their ECL performances: Ag^{s}/LDH/ITO > Au^{s}/LDH/ITO > Ag^{np}/LDH/ITO > Au^{np}/LDH/ITO (Fig. 1d). In other words, the larger upshift of d-band centers towards the Fermi level was associated with the higher ECL activity of the modified electrodes. The varied positions of the d-band center of metal species could be induced by the electronic metal–support interaction (EMSI),[33,34] which could regulate the electronic structure and the electron transfer ability of Ag or Au species. These results demonstrated the strength of ECL in identifying and screening the position of d-band centers of single-atomic and metallic catalysts.

Structural and morphological studies

To unveil the reason for this correlation, the structural and morphological features of these modified electrodes were studied. Taking the Ag species as an example, the typical characteristic diffraction peaks of LDH at 11.56°, 23.21° and 35.26° could be observed for Ag^{s}/LDH/ITO and Ag^{np}/LDH/ITO (Fig. S3†), demonstrating the presence of the periodically layered LDHs.[35] The characteristic diffraction peak of Ag nanoparticles at 38.28° could be observed for Ag^{np}/LDH/ITO and Ag^{np}/ITO. In contrast, no such peak could be observed for Ag^{s}/LDH/ITO, suggesting the absence of Ag nanoparticles. UV-vis spectra showed the surface plasma resonance peak at ∼460 nm for Ag^{np}/ITO, while this peak was absent for Ag^{s}/LDH/ITO (Fig. S4†). These results ruled out the aggregation of Ag in Ag^{s}/LDH/ITO and demonstrated the successfull preparation of monodispersed Ag single atoms on the LDH/ITO electrodes. Similarly, the localization of the single atomic Au on the LDH/ITO electrodes could be confirmed by the absence of the characteristic diffraction peak of Au nanoparticles in XRD patterns (Fig. S5†) and the surface plasma resonance peak in UV-vis spectra (Fig. S6†). The morphological characterization studies were performed to verify the presence of Ag and Au species in the as-prepared samples. The SEM images showed the vertically arranged CoAl/LDH arrays on the ITO substrate, with 1 μm in length and ∼20 nm in thickness (Fig. S7†). The high-angle annular dark-field scanning transmission electron microscopy (HAADF-STEM) image of Ag^{s}/LDH/ITO showed a number of isolated bright spots located on the CoAl/LDH, which can be attributed to the single atomic Ag (Fig. 2a). Furthermore, the mapping images showed that the Ag, Co and Al elements were uniformly distributed on the CoAl/LDH (Fig. 2b), validating the localization of single atomic Ag onto the LDH support. Similarly, bright spots ascribed to the single atomic Au could be observed on the surface of the CoAl/LDH (Fig. 2c and d), demonstrating the successful preparation of Au^{s}/LDH/ITO. Moreover, Au and Ag nanoparticles were mono-dispersed on the LDH support in Au^{np}/LDH/ITO and Ag^{np}/LDH/ITO, as observed from TEM images (Fig. S8†).

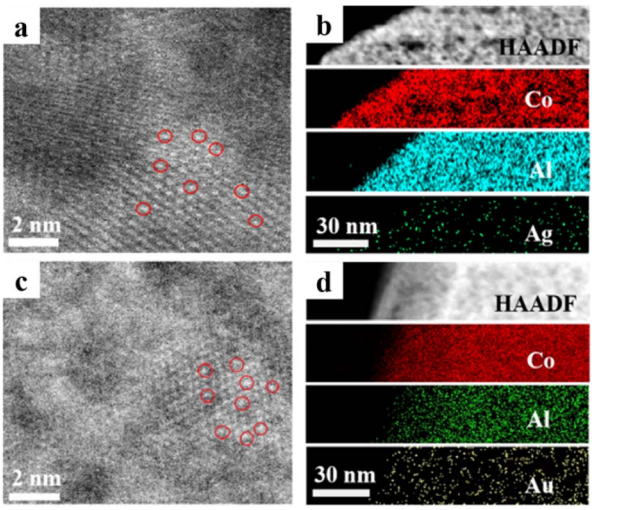

Fig. 2 (a) HAADF-STEM image and (b) STEM-EDS mapping images of Co, Al, and Ag for Ag^{s}/LDH/ITO; (c) HAADF-STEM image and (d) STEM-EDS mapping images of Co, Al, and Au for Au^{s}/LDH/ITO.

Open Access Article. Published on 07 October 2024. Downloaded on 2/8/2026 9:26:34 AM. This article is licensed under a Creative Commons Attribution-NonCommercial 3.0 Unported Licence.

Electronic structure studies

The electronic structure and local coordination of these modified electrodes were investigated by X-ray photoelectron spectroscopy (XPS). It can be observed that the binding energies of Ag $3d_{5/2}$ and Ag $3d_{3/2}$ were located at 367.5 and 373.5 eV for Ag^{np}/ITO (Fig. 3a), demonstrating the presence of metallic Ag^0.[36] These peaks shifted to higher binding energies of 367.8 and 373.9 eV in Ag^{np}/LDH/ITO. Furthermore, the peaks of Ag $3d_{5/2}$ for Ag^s/LDH/ITO shifted to 368.2 eV, demonstrating an intermediate valence between the metallic Ag^0 and Ag^+ ($0 < Ag^{\delta+} < +1$). Notably, the peaks were more inclined to Ag^+ in Ag^s/LDH/ITO, suggesting the strong interaction between single atomic Ag and LDHs, which may be responsible for the significant upshift of d-band centers to the Fermi level.[37] The O 1s spectra of the electrodes modified with Ag species were deconvoluted into three peaks at 533.8, 531.8, and 530.6 eV (Fig. 3b), ascribed to the oxygen in adsorbed molecular water (O_H), adsorbed oxygen (O_o), and lattice oxygen (O_{lat}), respectively.[38,39] The peaks indexed to O 1s in CoAl/LDH were shifted to a lower binding energy upon localization of Ag nanoparticles or single atoms. A new peak at 529.5 eV could be observed for Ag^s/LDH/ITO, suggesting the formation of Ag–O bonds.[40] Moreover, XPS spectra for Co 2p were studied to reveal the changes in the electronic structure of CoAl/LDH, and the core level Co 2p spectra were split into two peaks at 781.4/797.2 eV for Co^{2+} and 783.2/798.7 eV for Co^{3+} (Fig. 3c). These peaks of CoAl/LDH shifted to lower binding energies upon localization of Ag^{np} and Ag^s, accompanied by a significant decrease in the content of high-valent Co^{3+}. These variations indicated a possible electron transfer from Ag^s and Ag^{np} to CoAl/LDH through the O-bridge bimetal structure. Similar results could be observed for Au^s/LDH/ITO and Au^{np}/LDH/ITO electrodes. The peaks of Au $4f_{7/2}$ for Au^s/LDH/ITO were located at 84.6 eV (Fig. 3d), as an intermediate valence between the metallic Au^0 and Au^+.[41] In contrast, Au^{np}/ITO and Au^{np}/LDH/ITO showed peaks around 83.7 and 83.8 eV, respectively. The presence of the Au–O bond[42] could be observed as a new peak around 532.0 eV in the O 1s spectra for Au^s/LDH/ITO (Fig. 3e). Shifts to lower binding energies could also be observed in O 1s and Co 2p spectra for Au^s/LDH/ITO and Au^{np}/LDH/ITO, in comparison with CoAl/LDH (Fig. 3e and f). These findings suggested the partial electron transfer from Au^s and Au^{np} to the adjacent coordination due to the EMSI effect. In addition, Al 2p core-level spectra were deconvoluted into two peaks at 74.7 and 74.1 eV.[43] No obvious changes could be observed in the Al 2p spectra for all the modified electrodes (Fig. S9 and S10†), suggesting that Al atoms in LDH showed negligible effects on the interfacial electronic interactions.

Quantitative results from XPS spectra have addressed the differences between these modified electrodes. The ratios of Co^{3+}/Co^{2+} showed a slight decrease from 71.9% in CoAl/LDH to 70.3% in Ag^{np}/LDH/ITO and 68.4% in Au^{np}/LDH/ITO, while more significant reduction could be observed for 40.6% in Ag^s/LDH/ITO and 65.4% in Au^s/LDH/ITO (Table S1†). Such a phenomenon could be ascribed to the unique electronic structure and well-defined active sites of single atoms, exhibiting great potentials in enhancing the catalytic activity during an electrochemical reaction.[44,45] Moreover, the electronic structure of metal catalysts could be effectively regulated through the electronic metal–support interaction (EMSI).[46] It has been known that the EMSI effect is associated with the orbital rehybridization of metal catalysts and charge transfer across the metal–support interface.[47] Note that the rearrangement of electrons with a considerable EMSI effect is only confined to a couple of atomic layers at the metal–support interface.[48]

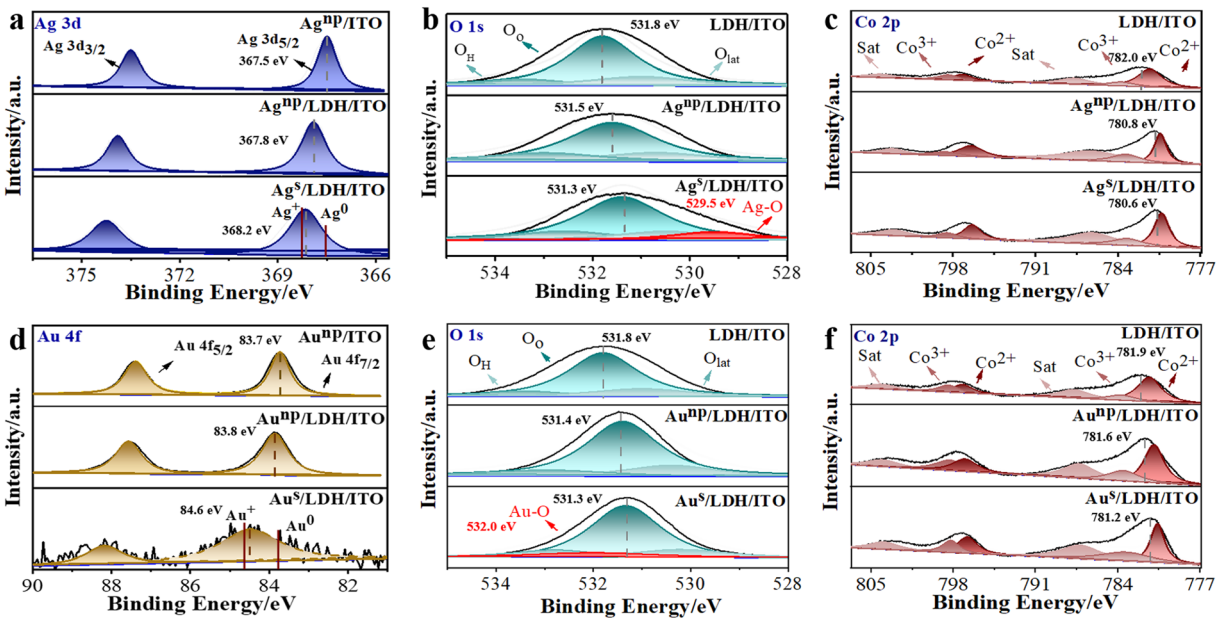

Fig. 3 High-resolution XPS spectra of (a) Ag 3d, (b) O 1s and (c) Co 2p for LDH/ITO, Ag^{np}/ITO, Ag^{np}/LDH/ITO and Ag^s/LDH/ITO; high-resolution XPS spectra of (d) Au 4f, (e) O 1s and (f) Co 2p for LDH/ITO, Au^{np}/ITO, Au^{np}/LDH/ITO and Au^s/LDH/ITO (the positions of the dotted line are marked in the diagram).

© 2024 The Author(s). Published by the Royal Society of Chemistry

Open Access Article. Published on 07 October 2024. Downloaded on 2/8/2026 9:26:34 AM. This article is licensed under a Creative Commons Attribution-NonCommercial 3.0 Unported Licence.

Accordingly, the stronger EMSI effect could be induced for single-atom catalysts than for the nanoparticles, leading to the modulated d state and the facilitated electron transfer from single-atom catalysts to LDH/ITO. Therefore, we will focus on the microstructural variations of these single atoms in the following discussions.

The average oxidation states of single atomic Ag and Au on the LDH/ITO have been calculated through the quantitative peak deconvolution and integration, and the oxidation states of single atomic Ag and Au on the LDH/ITO supports were estimated to be +0.9 and +0.7 eV, respectively (please see Table S2† for the detailed information and calculation process). As expected, electrons were transferred from Ag or Au single atoms to the LDH/ITO support due to the EMSI effect, and more electron transfer occurred for Ag^S/LDH/ITO with upshifted d-band centers. It is thus concluded that Ag single atoms with a higher oxidation state were energetically favorable for the adsorption and activation of oxygen species for the ECL reactions. Moreover, O 1s spectra showed that the contents of oxygen vacancies (O_o) for Ag^S/LDH/ITO and Au^S/LDH/ITO were 71.2% and 70.3%, respectively (Table S3†). The higher contents of oxygen vacancies in Ag^S/LDH/ITO indicated the stronger oxygen adsorption capacity, in accordance with the positions of the d-band centers. The Ag–O and Au–O bonds accounted for 7.5% and 6.0% in O 1s spectra for Ag^S/LDH/ITO and Au^S/LDH/ITO, suggesting the stronger metal–oxygen bonds in Ag^S/LDH/ITO for the electronic redistribution. Therefore, the data from XPS confirmed the upshifted d-band center of single atomic Ag and Au towards the Fermi level, in correlation with adsorption and activation abilities toward oxygen intermediates.

Ability to absorb, activate, and utilize the oxygen species

The redistributed electrons and oxidation state of metal species may affect their abilities to absorb, activate, and utilize the oxygen species during reaction. The oxygen adsorption ability at the modified electrodes was studied by O_2-temperature programmed desorption (O_2-TPD). It has been reported that the adsorbed oxygen changed from the physically adsorbed O_2 (desorbed below 200 °C) to the chemically adsorbed oxygen species (O_2^-/O^-, in the range of 200–400 °C) and eventually to the O_2^- in the lattice of the catalysts (higher than 400 °C).[49,50] LDH/ITO showed two oxygen desorption peaks at about 291 °C and 736 °C (Fig. 4a), corresponding to the chemically adsorbed oxygen species and lattice oxygen species, respectively. Upon localization of single atomic Ag and Au, the temperatures of these two peaks decreased to 270/634 °C for Au^S/LDH/ITO and 244/602 °C for Ag^S/LDH/ITO, suggesting the improved oxygen adsorption capacity of the modified electrodes. Note that compared to Au^S/LDH/ITO, Ag^S/LDH/ITO with upshifted d-band centers required a lower temperature to absorb oxygen species and showed stronger potential to produce active oxygen species.

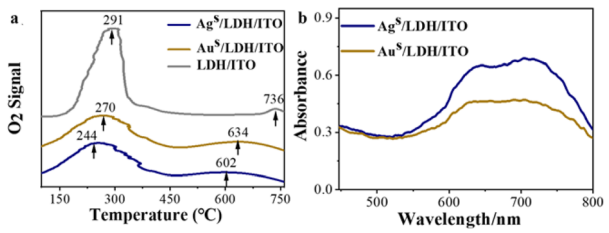

Fig. 4 (a) O_2-TPD pattern of LDH/ITO, Au^S/LDH/ITO and Ag^S/LDH/ITO electrodes; (b) UV-vis spectra of methyl hydrazone for the Ag^S/LDH/ITO and Au^S/LDH/ITO electrodes in KOH/DMSO solution.

These adsorbed oxygen species could be converted to ROS during the negative scan, such as superoxide ($O_2^{\bullet-}$), singlet oxygen ($^1O_2$), and hydroxyl radicals ($OH^\bullet$).[51] To validate the presence of these radicals, radical scavengers, such as *p*-benzoquinone (BQ, $O_2^{\bullet-}$ radical scavenger), isopropyl alcohol (IPA, $OH^\bullet$ radical scavenger) and NaN_3 ($^1O_2$ radical scavenger),[52] have been added to the luminol solution in the presence of different electrodes. It can be observed that the ECL signals during the scan from −0.8 to 0 V were quenched by BQ, IPA and NaN_3 at Ag^S/LDH/ITO and Au^S/LDH/ITO electrodes (Fig. S11 and S12†), indicating the significance of $O_2^{\bullet-}$, $OH^\bullet$ and $^1O_2$ for the ECL emission. Particularly, the ECL signals were significantly quenched for 99% at Ag^S/LDH/ITO and 97% at Au^S/LDH/ITO when the $O_2^{\bullet-}$ was scavenged by BQ (Table S4†). These results suggested that $O_2^{\bullet-}$ was the dominant ROS that contributed to the impressive cathodic emission of the luminol-dissolved O_2 ECL system. The quantity of $O_2^{\bullet-}$ was further evaluated by nitro blue tetrazolium chloride (NBT),[53] and the amount of oxidation product methyl hydrazone was recorded by UV-vis spectroscopy (Fig. 4b). Notably, the absorbance of the oxidized product was higher for Ag^S/LDH/ITO than for Au^S/LDH/ITO, illustrating the excellent ability of Ag^S/LDH/ITO to catalyse the generation of $O_2^{\bullet-}$ than Au^S/LDH/ITO did. These results demonstrate that $O_2^{\bullet-}$ played vital roles in determining the ECL signals,[47] due to its functionality to oxidize the luminol anions ($L^{\bullet-}$) to form excited-state 3-aminophthalate (AP_2^{2-*}) for the ECL emissions (Scheme S1†). Furthermore, we measured the ECL in the range from 0 to +0.8 V and quantified the generated $O_2^{\bullet-}$ in the anodic ECL reaction for luminol. Upon the addition of BQ, most of the ECL signals at Ag^S/LDH/ITO and Au^S/LDH/ITO were quenched, and the absorbance values of the oxidation products of NBT were almost the same at the Au^S/LDH/ITO and Ag^S/LDH/ITO electrodes (Fig. S13†). These results suggested the generation of similar amounts of $O_2^{\bullet-}$ during the anodic ECL reaction at the Au^S/LDH/ITO and Ag^S/LDH/ITO electrodes, responsible for the similar amounts of AP_2^{-*} and ECL emissions (Scheme S1†). Therefore, we have employed the cathodic ECL as the indicator, and Ag^S/LDH/ITO showed superior ability in absorbing and activating the ROS to achieve the enhanced catalytic performances and cathodic ECL intensities.

Mechanisms to spot the d-band centers by the cathodic luminol ECL

Electrochemical impedance spectroscopy (EIS) was performed on the modified electrodes in 5.0 mmol L^{-1} $K_3[Fe(CN)_6]$/$K_4[Fe(CN)_6]$ (0.1 mol L^{-1} KCl) from 0.1 Hz to 100 kHz. An equipped equivalence circuit is shown as the inset in Fig. S14,† where R_s, R_{ct}, C_{dl}, and W represent the resistance of solution, charge transfer resistance, double layer capacitance, and the

Open Access Article. Published on 07 October 2024. Downloaded on 2/8/2026 9:26:34 AM. This article is licensed under a Creative Commons Attribution-NonCommercial 3.0 Unported Licence.

Warburg constant, respectively. The charge transfer resistance (R_{ct}) from the Nyquist plot followed the trend: LDH/ITO (82.4 Ω) > ITO (69.6 Ω) > Au^S/LDH/ITO (54.5 Ω) > Ag^S/LDH/ITO (46.9 Ω), indicating the higher electron transfer ability of Ag^S/LDH/ITO than that of Au^S/LDH/ITO (Fig. S14†). The oxygen reduction reaction (ORR) is a critical step to generate ROS through electrochemical reactions and is highly correlated with the efficiency of the luminol ECL emission.[51] The linear sweep voltammetry (LSV) curves showed that Ag^S/LDH/ITO possessed more positive onset potential and a higher ORR current than Au^S/LDH/ITO did (Fig. 5a), indicating the effectively activated catalytic activity of Ag^S/LDH/ITO. This result was consistent with the ECL performance of the modified electrodes. Tafel slope curves further showed the values of 164.4 mV dec^{-1} for Ag^S/LDH/ITO and 208.4 mV dec^{-1} for Au^S/LDH/ITO (Fig. 5b). The smaller Tafel slope of Ag^S/LDH/ITO indicated the faster electron transport and superior kinetics for the ORR.[54] It has been known that the ORR kinetics process can proceed *via* either a $2e^-$ ($O_2 + H_2O + 2e^- \; HO_2^- + OH^-$) or $4e^-$ ($O_2 + 2H_2O + 4e^- \; 4OH^-$) pathway, which is dependent on the propensity to break the O–O bond during the ORR process.[55] To figure out the pathways of the ORR process, the electron transfer number (n) involved in the ORR process was studied according to the Koutecky–Levich (K–L) plots (Fig. S15 and S16†). The number of electrons transferred during the ORR was different for different modified electrodes: the calculated n was 3.53 for Ag^S/LDH/ITO and 2.46 for Au^S/LDH/ITO (Fig. 5c). Such a result suggested that the $4e^-$ pathway of the ORR process was preferred in the presence of Ag^S/LDH/ITO, and Ag^S/LDH/ITO exhibited better ORR electrocatalytic activity and reaction kinetics than Au^S/LDH/ITO did. Note that the $4e^-$ reaction pathway involves more ROS, beneficial for the ECL reaction and emission enhancement.[56] In consequence, these findings well explained the significantly enhanced ECL signals by Ag^S/LDH/ITO.

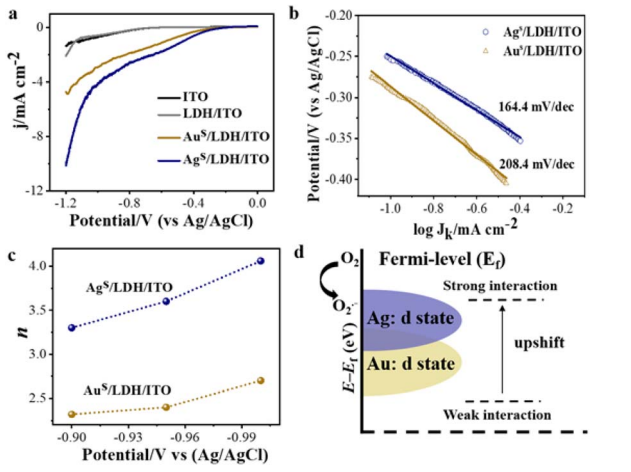

Fig. 5 (a) Current density (j)–voltage curves in O_2-saturated PBS (pH = 7.5) at ITO, LDH/ITO, Au^S/LDH/ITO and Ag^S/LDH/ITO electrodes; (b) Tafel slope curves of Ag^S/LDH/ITO and Au^S/LDH/ITO electrodes; (c) average electron transfer numbers (n) calculated from the K–L equation during the oxygen reduction reaction; (d) schematic illustration of the d-band center shift from the Fermi level for single atomic Ag and Au.

The d-band model proposed by Nørskov was used to explain the electronic structure and thus the catalytic performances for these modified electrodes. Upon adsorption of O_2 on the surface of the modified electrodes, bonding and antibonding states were formed between the p-band of adsorbate and d-band of metal species.[1] The d-band centers of the metal species were shifted as a consequence. The closer location of d-band centers of Ag^S/LDH/ITO to the Fermi level than that of Au^S/LDH/ITO resulted in the strengthened bonding interaction between Ag single atoms and oxygen intermediates (Fig. 5d). Therefore, much stronger oxygen reduction ability could be acquired for Ag^S/LDH/ITO, facilitating the generation of ROS for the ORR process and the promoted ECL emission of luminol. Therefore, the ECL signals showed the strength and accuracy to evaluate the d-band centers of single-atom catalysts in a sensitive approach.

Finally, we explored the universality of the proposed ECL strategy by other single-atom catalysts. First, Cu, which is listed in the same main group of Au and Ag, was prepared as single atomic Cu on LDH/ITO (labelled as Cu^S/LDH/ITO). XRD and UV-vis spectra have excluded the appearance of Cu nanoparticles in Cu^S/LDH/ITO (Fig. S17 and S18†). The HAADF-STEM image showed the uniform distribution of bright spots, which were ascribed to the single atomic Cu (Fig. S19†). The UPS valence-band spectra showed that the energy of d-band centers of Cu^S/LDH/ITO was located at −4.46 eV (Fig. S20†), and the ECL measurements showed that the cathodic ECL intensity of Cu^S/LDH/ITO was about 1200 a.u. (Fig. S21†). Second, single atomic Fe was prepared, as validated using the XRD spectra, UV-vis spectra and HAADF-STEM images (Fig. S22–S24†). The as-prepared Fe^S/LDH/ITO exhibited the energy of d-band centers at −4.97 eV (Fig. S25†) and the cathodic ECL intensity of 400 a.u. (Fig. S26†). As expected, both the ECL intensities and the positions of d-band centers for these single-atom catalysts followed the same trend: Ag^S/LDH/ITO > Au^S/LDH/ITO > Cu^S/LDH/ITO > Fe^S/LDH/ITO (Fig. S27†). Therefore, we validated the universality of the proposed intermediate-boosted ECL in spotting the d-band centers of single-atom catalysts.

Conclusions

In summary, we have proposed oxygen intermediate-boosted ECL signals for an accurate and sensitive evaluation of the d-band centers of single-atom catalysts. Ag, Au, Cu and Fe single atoms with different d-band centers were localized onto CoAl/LDH supports as catalysts. In accordance with the largest upshift of d-band centers towards the Fermi level, Ag^S/LDH/ITO displayed a notable oxygen adsorption capacity and remarkable catalytic activity to generate ROS, leading to the strongest ECL emissions from luminol reactions. The variation tendency of the ECL signals and the positions of d-band centers were highly correlated: Ag^S/LDH/ITO > Au^S/LDH/ITO > Cu^S/LDH/ITO > Fe^S/LDH/ITO. Such a correlation was also adapted for the nanoparticle catalysts such as Ag and Au nanoparticles, validating the higher catalytic efficiency of single atoms than that of nanoparticles. The proposed ECL strategy featured some advantages, such as high sensitivity, good accuracy, and simple

© 2024 The Author(s). Published by the Royal Society of Chemistry

Open Access Article. Published on 07 October 2024. Downloaded on 2/8/2026 9:26:34 AM. This article is licensed under a Creative Commons Attribution-NonCommercial 3.0 Unported Licence.

sampling and analysing processes. Distinguishable signals with large variations could be acquired for the metal catalysts through an ECL cell for the luminol reaction. These advantages revealed that the proposed ECL strategy is an applicable and versatile method to evaluate the d-band centers for the metal catalysts. Moreover, the proposed strategy has also deepened the understanding of the d-band centers in determining the catalytic efficiencies for catalysts. This prospective methodology could be further applied to study and tailor the electronic structures for catalysts.

Data availability

The data supporting the findings of this study are available within the article and ESI.† All other relevant source data are available from the corresponding authors upon reasonable request.

Author contributions

Chao Lu and Rui Tian conceived the experiments. Ruyu Xie and Kaitao Li carried out the experiments. Ruyu Xie, Rui Tian and Chao Lu contributed to the data analysis and writing of this manuscript.

Conflicts of interest

There are no conflicts to declare.

Acknowledgements

This work was supported by the National Natural Science Foundation of China (U22A20397 and 22374008) and Beijing Natural Science Foundation (2222018).

Notes and references

1 B. Hammer and J. K. Nørskov, *Surf. Sci.*, 1995, **343**, 211–220.
2 T. Tang, X. Bai, Z. Wang and J. Guan, *Chem. Sci.*, 2024, **15**, 5082–5112.
3 A. Ruban, B. Hammer, P. Stoltze, H. L. Skriver and J. K. Nørskov, *J. Mol. Catal. A: Chem.*, 1997, **115**, 421–429.
4 Z. Li, Z. L. Tian, H. Cheng, T. Wang, W. Zhang, Y. Lu, Y. Q. Lai and G. J. He, *Energy Storage Mater.*, 2023, **59**, 102764.
5 H. Sun, M. F. Wang, X. C. Du, Y. Jiao, S. S. Liu, T. Qian, Y. C. Yan, C. Liu, M. Liao, Q.-H. Zhang, L. X. Meng, L. Gu, J. Xiong and C. L. Yan, *J. Mater. Chem. A*, 2019, **7**, 20952–20957.
6 L. L. Li, Y.-F. Jiang, T. H. Zhang, H. F. Cai, Y. L. Zhou, B. Y. Lin, X. Y. Lin, Y. Zheng, L. R. Zheng, X. Y. Wang, C.-Q. Xu, C. Au, L. L. Jiang and J. Li, *Chem*, 2022, **8**, 749–768.
7 H. Liu, C. Wang, C. Liu, X. Zong, Y. F. Wang, X. X. Huang, Z. Z. Hu and Z. Q. Zhang, *ACS Appl. Mater. Interfaces*, 2023, **15**, 29110–29119.
8 X. Li, J. Liu, Q. Cai, Z. Kan, S. Liu and J. Zhao, *J. Colloid Interface Sci.*, 2022, **628**, 331–342.
9 X. Y. Tian, R. J. Ren, F. Y. Wei, J. J. Pei, Z. B. Zhuang, L. Zhuang and W. C. Sheng, *Nat. Commun.*, 2024, **15**, 76.
10 Y. Shi, Z.-R. Ma, Y.-Y. Xiao, Y.-C. Yin, W.-M. Huang, Z.-C. Huang, Y.-Z. Zheng, F.-Y. Mu, R. Huang, G.-Y. Shi, Y.-Y. Sun, X.-H. Xia and W. Chen, *Nat. Commun.*, 2021, **12**, 3021.
11 X. Wu, F. Chen, N. Zhang, Y. Lei, Y. Jin, A. Qaseem and R. L. Johnston, *Small*, 2017, **13**, 1603387.
12 Q. Yuan, J. Zhao, D. H. Mok, Z. Zheng, Y. Ye, C. Liang, L. Zhou, S. Back and K. Jiang, *Nano Lett.*, 2022, **22**, 1257–1264.
13 Z. Chen, Y. Song, J. Cai, X. Zheng, D. Han, Y. Wu, Y. Zang, S. Niu, Y. Liu, J. Zhu, X. Liu and G. Wang, *Angew. Chem., Int. Ed.*, 2018, **57**, 5076–5080.
14 K. Artyushkova, A. Serov, H. Doan, N. Danilovic, C. B. Capuano, T. Sakamoto, H. Kishi, S. Yamaguchi, S. Mukerjee and P. Atanassov, *J. Electron Spectrosc. Relat. Phenom.*, 2019, **231**, 127–139.
15 J. Mahoney, C. Monroe, A. M. Swartley, M. G. Ucak-Astarlioglu and C. A. Zoto, *Spectrosc. Lett.*, 2020, **53**, 726–736.
16 Q. Hu, K. Gao, X. Wang, H. Zheng, J. Cao, L. Mi, Q. Huo, H. P. Yang, J. Liu and C. He, *Nat. Commun.*, 2022, **13**, 3958.
17 S. F. Douman, D. Collins, L. R. Cumba, S. Beirne, G. G. Wallace, Z. L. Yue, E. I. Iwuoha, F. Melinato, Y. Pellegrin and R. J. Forster, *Chem. Commun.*, 2021, **57**, 4642–4645.
18 M. Feng, A. L. Dauphin, L. Bouffier, F. Zhang, Z. Wang and N. Sojic, *Anal. Chem.*, 2021, **93**, 16425–16431.
19 Y. H. Huang, R. Y. Xie, K. T. Li, R. Tian, Y. Lin and C. Lu, *ACS Appl. Mater. Interfaces*, 2023, **15**, 1610–1618.
20 Y. P. Dong, J. Wang, Y. Peng and J. J. Zhu, *J. Electroanal. Chem.*, 2016, **781**, 109–113.
21 D. Wei, L. Chen, H. Zhao, L. Tian, S. Ramakrishna and D. Ji, *ACS Appl. Nano Mater.*, 2023, **6**, 11061–11069.
22 X. Zhou, J. J. Gao, Y. X. Hu, Z. Y. Jin, K. L. Hu, K. M. Reddy, Q. H. Yuan, X. Lin and H.-J. Qiu, *Nano Lett.*, 2022, **22**, 3392–3399.
23 Z. Zhang, C. Feng, C. Liu, M. Zuo, L. Qin, X. Yan, Y. Xing, H. Li, R. Si, S. Zhou and J. Zeng, *Nat. Commun.*, 2020, **11**, 1215.
24 E. D. Boyes, A. P. LaGrow, M. R. Ward, R. W. Mitchell and P. L. Gai, *Acc. Chem. Res.*, 2020, **53**, 390–399.
25 N. Acerbi, S. C. E. Tsang, G. Jones, S. Golunski and P. Collier, *Angew. Chem., Int. Ed.*, 2013, **52**, 7737–7741.
26 W. Miao, *Chem. Rev.*, 2008, **108**, 2506–2553.
27 A. J. Marenco, D. B. Pedersen, S. Wang, M. W. P. Petryk and H. B. Kraatz, *Analyst*, 2009, **134**, 2021–2027.
28 S. A. Chala, M.-C. Tsai, W.-N. Su, K. B. Ibrahim, B. Thirumalraj, T.-S. Chan, J.-F. Lee, H. J. Dai and B.-J. Hwang, *ACS Catal.*, 2019, **9**, 117–129.
29 R. Zou, Y. J. Lin and C. Lu, *Anal. Chem.*, 2021, **93**, 2678–2686.
30 H. Cui, Y. Xu and Z. F. Zhang, *Anal. Chem.*, 2004, **76**, 4002–4010.
31 Y. H. Huang, R. Zou, Y. J. Lin and C. Lu, *Anal. Chem.*, 2021, **93**, 11291–11297.
32 X. L. Huo, H. Yang, M.-X. Li, W. Zhao, J.-J. Xu, Y. Wang, X.-L. Luo and H.-Y. Chen, *Nanoscale*, 2018, **10**, 19224–19230.

© 2024 The Author(s). Published by the Royal Society of Chemistry

Open Access Article. Published on 07 October 2024. Downloaded on 2/8/2026 9:26:34 AM. This article is licensed under a Creative Commons Attribution-NonCommercial 3.0 Unported Licence.

33 J. Wei, K. Xiao, Y. Chen, X. P. Guo, B. Huang and Z. Q. Liu, *Energy Environ. Sci.*, 2022, **15**, 4592–4600.
34 J. Li, Q. Q. Guan, H. Wu, W. Liu, Y. Lin, Z. H. Sun, X. X. Ye, X. S. Zheng, H. B. Pan, J. F. Zhu, S. Chen, W. H. Zhang, S. Q. Wei and J. L. Lu, *J. Am. Chem. Soc.*, 2019, **141**, 14515–14519.
35 Y. Hou, J. Feng, R. Tian, C. Lu and X. Duan, *Angew. Chem., Int. Ed.*, 2023, **62**, e202307573.
36 N. Zhang, X. Zhang, L. Tao, P. Jiang, C. Ye, R. Lin, Z. Huang, A. Li, D. Pang, H. Yan, Y. Wang, P. Xu, S. An, Q. Zhang, L. Liu, S. Du, X. Han, D. Wang and Y. Li, *Angew. Chem., Int. Ed.*, 2021, **60**, 6170–6176.
37 X. Wang, S. Li, Z. Yuan, Y. Sun, Z. Tang, X. Gao, H. Zhang, J. Li, S. Wang, D. Yang, J. Xie, Z. Yang and Y.-M. Yan, *Angew. Chem., Int. Ed.*, 2023, **62**, e202303794.
38 H. Zeng, L. Deng, H. Zhang, C. Zhou and Z. Shi, *J. Hazard. Mater.*, 2020, **400**, 123297.
39 L. Wu, J. Hong, Q. Zhang, B. Y. Chen, J. Wang and Z. Dong, *Chem. Eng. J.*, 2020, **385**, 123620.
40 F.-F. Zhang, C.-Q. Cheng, J.-Q. Wang, L. Shang, Y. Feng, Y. Zhang, J. Mao, Q.-J. Guo, Y.-M. Xie, C.-K. Dong, Y.-H. Cheng, H. Liu and X.-W. Du, *ACS Energy Lett.*, 2021, **6**, 1588–1595.
41 L. J. Lei, H. Liu, Z. W. Wu, Z. F. Qin, G. F. Wang, J. Y. Ma, L. Luo, W. B. Fan and J. G. Wang, *ACS Appl. Nano Mater.*, 2019, **2**, 5214–5223.
42 P. Kundu, N. Singhania, G. Madras and N. Ravishankar, *Dalton Trans.*, 2012, **41**, 8762–8766.
43 L. Rosenberger, R. Baird, E. McCullen, G. Auner and G. Shreve, *Surf. Interface Anal.*, 2008, **40**, 1254–1261.
44 C. P. Wang, S. J. Mao, Z. Wang, Y. Z. Chen, W. T. Yuan, Y. Ou, H. Zhang, Y. T. Gong, Y. Wang, B. B. Mei, Z. Jiang and Y. Wang, *Chem*, 2020, **6**, 752–765.
45 J. Li, M. F. Stephanopoulos and Y. Xia, *Chem. Rev.*, 2020, **120**, 11699–11702.
46 A. Bruix, J. A. Rodriguez, P. J. Ramírez, S. D. Senanayake, J. Evans, J. B. Park, D. Stacchiola, P. Liu, J. Hrbek and F. Illas, *J. Am. Chem. Soc.*, 2012, **134**, 8968–8974.
47 G. Vayssilov, Y. Lykhach, A. Migani, T. Staudt, G. Petrova, N. Tsud, T. Skála, A. Bruix, F. Illas and K. Prince, *Nat. Mater.*, 2011, **10**, 310–315.
48 T. W. van Deelen, C. Hernández Mejía and K. P. de Jong, *Nat. Catal.*, 2019, **2**, 955–970.
49 P. Li, C. He, J. Cheng, C. Y. Ma, B. J. Dou and Z. P. Hao, *Appl. Catal., B*, 2011, **101**, 570–579.
50 W. Deng, Q. Tang, S. Huang, L. Zhang, Z. Jia and L. Guo, *Appl. Catal., B*, 2020, **278**, 119336.
51 H. Xia, X. L. Zheng, J. Li, L. G. Wan, Y. Xue, C. Peng, Y. C. Han, Y. Wang, S. J. Guo, J. Wang and E. K. Wang, *J. Am. Chem. Soc.*, 2022, **144**, 7741–7749.
52 W. Gu, H. J. Wang, L. Jiao, Y. Wu, Y. X. Chen, L. Y. Hu, J. M. Gong, D. Du and C. Zhu, *Angew. Chem., Int. Ed.*, 2020, **59**, 3534–3538.
53 R.-H. Liu, S.-Y. Fu, H.-Y. Zhan and L. A. Lucia, *Ind. Eng. Chem. Res.*, 2009, **48**, 9331–9334.
54 W. Wang, Y. Liu, J. Li, J. Luo, L. Fu and S. Chen, *J. Mater. Chem. A*, 2018, **6**, 14299–14306.
55 J. Hu, W. Liu, C. Xin, J. Guo, X. Cheng, J. Weai, C. Hao, G. Zhang and Y. Shi, *J. Mater. Chem. A*, 2021, **9**, 24803–24829.
56 W. Gu, X. S. Wang, J. Wen, S. Y. Cao, L. Jiao, Y. Wu, X. Q. Wei, L. R. Zheng, L. Y. Hu, L. Z. Zhang and C. Z. Zhu, *Anal. Chem.*, 2021, **93**, 8663–8670.

© 2024 The Author(s). Published by the Royal Society of Chemistry